

# Measurements of top-quark pair asymmetries in the dilepton final state at $\sqrt{s} = 7$ TeV

D. Barge, C. Campagnari, A. George, D. Kovalskyi, V. Krutelyov

*University of California, Santa Barbara*

W. Andrews, G. Cerati, D. Evans, F. Golf, I. Macneill, S. Padhi, Y. Tu, V. Wellke, F. Würthwein,  
A. Yagil, J. Yoo

*University of California, San Diego*

L. Bauerdick, K. Burkett, I. Fisk, Y. Gao, O. Gutsche, B. Hooberman, S. Jindariani, J. Linacre,  
V. Martinez Outschoorn

*Fermi National Accelerator Laboratory, Batavia, Illinois*

## Abstract

Measurements of several dilepton asymmetries in  $t\bar{t} \rightarrow \ell^+\ell^-$  events are performed in a data sample corresponding to a total integrated luminosity of  $5.0 \text{ fb}^{-1}$  collected by the CMS experiment in pp collisions at a centre-of-mass energy of 7 TeV at the LHC. <sup>1)</sup> The observables include the lepton charge and the top charge asymmetry, the lepton azimuthal asymmetry, as well as the top polarization and spin correlation. In view of a more significant excess reported in related observables at the Tevatron for high  $t\bar{t}$  system mass, the results are also given for  $t\bar{t}$  system mass above 450 GeV. The measured values of these observables are found in agreement with their standard model expectations. These results are used to constrain contribution from axigluon production as well as from a t-channel W' exchange.

---

<sup>1)</sup> Disclaimer: the numbers in the note are not final and may slightly change as we finalize the analysis. Systematics are discussed in the corresponding section but are not yet included in the final result.

# Contents

<b>1</b>	<b>Introduction</b>	<b>2</b>
<b>2</b>	<b>Datasets, Triggers, Luminosity</b>	<b>2</b>
<b>3</b>	<b>Event Preselection</b>	<b>4</b>
3.1	Event Cleanup . . . . .	4
3.2	Muon Selection . . . . .	4
3.3	Electron Selection . . . . .	5
3.4	Trigger Selection . . . . .	5
<b>4</b>	<b>Trigger efficiency</b>	<b>6</b>
<b>5</b>	<b><math>b</math>-tagging Scale Factor</b>	<b>6</b>
<b>6</b>	<b>Observables</b>	<b>6</b>
<b>7</b>	<b>Preselection yields: Data/MC Comparison</b>	<b>7</b>
<b>8</b>	<b>Background Estimation</b>	<b>8</b>
8.1	Fake lepton background estimation . . . . .	10
8.2	Drell-Yan background estimation . . . . .	10
8.3	Remaining backgrounds . . . . .	10
<b>9</b>	<b>Signal region</b>	<b>11</b>
9.1	Signal region $I$ . . . . .	11
9.2	Signal region $II$ . . . . .	14
<b>10</b>	<b>Unfolding</b>	<b>14</b>
10.1	Binning . . . . .	16
10.2	Acceptance Effects . . . . .	16
10.3	Smearing Effects . . . . .	16
10.4	Linearity Tests . . . . .	18
<b>11</b>	<b>Systematics</b>	<b>21</b>
<b>12</b>	<b>Results</b>	<b>21</b>
	<b>Appendix A Fakeable Object Definitions</b>	<b>25</b>
	<b>Appendix B Data and MC comparison for the preselection</b>	<b>25</b>

# 1 Introduction

Measurements of the  $t\bar{t}$  forward-backward asymmetry ( $A_{fb}$ ) from the Tevatron have led to increased interest in asymmetries in top quark production from both experimentalists and theorists. The results from CDF [1], confirmed later by D0 [2], show a discrepancy between the measured value of  $A_{fb}$  and the predicted value from the standard model (SM). Recent results from CDF [3] report a greater than  $3\sigma$  discrepancy for events with large  $t\bar{t}$  invariant mass.

There are many models of new physics that predict larger values of  $A_{fb}$  than in the standard model. This often arises from interference between the standard model and the new physics, where typically top quarks are produced in the exchange of some new heavy particle. Any measurement of  $A_{fb}$  is thus potentially a search for evidence of new physics.

Because the Tevatron is a  $p\bar{p}$  collider, there is a natural definition for an asymmetry based on the incoming partons. While the LHC is a symmetric  $pp$  collider, it is still possible to measure asymmetries in top quark production. A recent paper by Krohn, Liu, Shelton, and Wang [4] suggests five different observables that can be studied. These include purely leptonic observables (the leptonic charge asymmetry and the azimuthal asymmetry) and observables that require reconstruction of the top decay (the charge asymmetry, polarization, and spin correlation).

This note presents a measurement of these asymmetries in top quark pair production using the full 2011 data at  $\sqrt{s} = 7$  TeV, corresponding to an integrated luminosity of  $5.0 \text{ fb}^{-1}$ . Dilepton decays of the  $t\bar{t}$  pair are used, and the asymmetries are measured for both the full sample and for events with a  $t\bar{t}$  invariant mass  $m_{t\bar{t}} \geq 450 \text{ GeV}/c^2$ . Because the reconstructed asymmetries are shaped by the reconstruction efficiency and resolution, we apply an unfolding technique to recover the parton-level distributions which can be compared with theoretical predictions.

This note is organized as follows: The datasets and triggers used for the analysis are described in Sec. 2, the analysis pre-selection is described in Sec. 3, and the trigger efficiencies are listed in Sec. 4. The five observables that we will study are defined in Sec. 6. Comparisons of the observed yields in data and simulation are shown at the pre-selection level in Sec. 7 and in the signal regions in Sec. 9. Background estimates are listed in Sec. 8. The procedure to unfold the observed distributions back to the parton level is presented in Sec. 10. Systematic uncertainties are evaluated in Sec. 11, and then final results are presented in Sec. 12.

## 2 Datasets, Triggers, Luminosity

$5.0 \text{ fb}^{-1}$  of data was analyzed, corresponding to the events included in the May10ReReco, Aug5ReReco and prompt Reco json files:

- Cert\_160404-163869\_7TeV\_May10ReReco\_Collisions11\_JSON\_v3.txt
- Cert\_170249-172619\_7TeV\_ReReco5Aug\_Collisions11\_JSON\_v3.txt
- Cert\_160404-180252\_7TeV\_PromptReco\_Collisions11\_JSON.txt

We use data reconstructed in CMSSW 4.2.X and Summer11 Monte Carlo reconstructed in CMSSW 4.2.X. We also use a Fall11 sample of MC@NLO  $t\bar{t}$  events, which is not available in Summer11.

The data samples were collected with high  $p_T$  dilepton triggers:

- High  $p_T$  DoubleElectron
  - /DoubleElectron/Run2011B-PromptReco-v1/AOD
  - /DoubleElectron/Run2011A-PromptReco-v6/AOD
  - /DoubleElectron/Run2011A-05Aug2011-v1/AOD
  - /DoubleElectron/Run2011A-PromptReco-v4/AOD
  - /DoubleElectron/Run2011A-May10ReReco-v1/AOD
- High  $p_T$  DoubleMu

- 46        - /DoubleMu/Run2011B-PromptReco-v1/AOD
- 47        - /DoubleMu/Run2011A-PromptReco-v6/AOD
- 48        - /DoubleMu/Run2011A-05Aug2011-v1/AOD
- 49        - /DoubleMu/Run2011A-PromptReco-v4/AOD
- 50        - /DoubleMu/Run2011A-May10ReReco-v1/AOD

51    • High  $p_T$  MuEG

- 52        - /MuEG/Run2011B-PromptReco-v1/AOD
- 53        - /MuEG/Run2011A-PromptReco-v6/AOD
- 54        - /MuEG/Run2011A-05Aug2011-v1/AOD
- 55        - /MuEG/Run2011A-PromptReco-v4/AOD
- 56        - /MuEG/Run2011A-May10ReReco-v1/AOD

57    The MC samples are listed with the name and the cross section:

- 58        • TTJets\_TuneZ2\_7TeV-madgraph-tauola\_Summer11-PU\_S4\_START42\_V11-v1 , 154 pb
- 59
- 60        • TTto2L2Nu2B\_7TeV-powheg-pythia6\_Summer11-PU\_S4\_START42\_V11-v1 , 16.5 pb
- 61
- 62        • /TT\_TuneZ2\_7TeV-mcatnlo/Fall11-PU\_S6\_START42\_V14B-v1/AODSIM , 154 pb
- 63
- 64        • T\_TuneZ2\_tW-channel\_7TeV-madgraph\_Summer11-PU\_S4\_START42\_V11-v1 , 7.87 pb
- 65
- 66        • T\_TuneZ2\_t-channel\_7TeV-madgraph\_Summer11-PU\_S4\_START42\_V11-v1 , 41.92 pb
- 67
- 68        • T\_TuneZ2\_s-channel\_7TeV-madgraph\_Summer11-PU\_S4\_START42\_V11-v1 , 3.19 pb
- 69
- 70        • Tbar\_TuneZ2\_tW-channel\_7TeV-madgraph\_Summer11-PU\_S4\_START42\_V11-v1 , 7.87 pb
- 71
- 72        • Tbar\_TuneZ2\_t-channel\_7TeV-madgraph\_Summer11-PU\_S4\_START42\_V11-v1 , 22.65 pb
- 73
- 74        • Tbar\_TuneZ2\_s-channel\_7TeV-madgraph\_Summer11-PU\_S4\_START42\_V11-v1 , 1.44 pb
- 75
- 76        • WJetsToLNu\_TuneZ2\_7TeV-madgraph-tauola\_Summer11-PU\_S4\_START42\_V11-v1 , 31314 pb
- 77
- 78        • DYJetsToLL\_TuneD6T\_M-50\_7TeV-madgraph-tauola\_Summer11-PU\_S4\_START42\_V11-v1 , 3048 pb
- 79
- 80        • DYToEE\_M-20\_CT10\_TuneZ2\_7TeV-powheg-pythia\_Summer11-PU\_S4\_START42\_V11-v1 , 1666 pb
- 81
- 82        • DYToMuMu\_M-20\_CT10\_TuneZ2\_7TeV-powheg-pythia\_Summer11-PU\_S4\_START42\_V11-v1 , 1666 pb
- 83
- 84        • DYToTauTau\_M-20\_CT10\_TuneZ2\_7TeV-powheg-pythia-tauola\_Summer11-PU\_S4\_START42\_V11-v1 , 1666 pb
- 85
- 86        • DYToEE\_M-10To20\_TuneZ2\_7TeV-pythia6\_Summer11-PU\_S4\_START42\_V11-v1 , 3319.61 pb
- 87
- 88        • DYToMuMu\_M-10To20\_TuneZ2\_7TeV-pythia6\_Summer11-PU\_S4\_START42\_V11-v1 , 3319.61 pb
- 89
- 90        • DYToTauTau\_M-10To20\_CT10\_TuneZ2\_7TeV-powheg-pythia-tauola\_Summer11-PU\_S4\_START42\_V11-v2 , 3319.61
- 91        pb
- 92

- 93 • WWJetsTo2L2Nu\_TuneZ2\_7TeV-madgraph-tauola\_ummer11-PU\_S4\_START42\_V11-v1, 4.783 pb
- 94
- 95 • WZJetsTo2L2Q\_TuneZ2\_7TeV-madgraph-tauola\_Summer11-PU\_S4\_START42\_V11-v1, 1.786 pb
- 96
- 97 • WZJetsTo3LNu\_TuneZ2\_7TeV-madgraph-tauola\_Summer11-PU\_S4\_START42\_V11-v1, 0.856 pb
- 98
- 99 • ZZJetsTo2L2Nu\_TuneZ2\_7TeV-madgraph-tauola\_Summer11-PU\_S4\_START42\_V11-v1, 0.30 pb
- 100
- 101 • ZZJetsTo2L2Q\_TuneZ2\_7TeV-madgraph-tauola\_Summer11-PU\_S4\_START42\_V11-v1, 1.0 pb
- 102
- 103 • ZZJetsTo4L\_TuneZ2\_7TeV-madgraph-tauola/\_ummer11-PU\_S4\_START42\_V11-v1, 0.076 pb
- 104

### 105 3 Event Preselection

106 The purpose of the preselection is to reject backgrounds other than  $t\bar{t} \rightarrow$  dileptons. We compare the  
 107 kinematical properties of this sample with expectations from MC.

108 The preselection is based on the  $t\bar{t}$  cross section analysis [14]. We select events with two opposite sign,  
 109 well-identified and isolated leptons ( $ee$ ,  $e\mu$ , or  $\mu\mu$ ) with  $p_T > 20$  GeV/ $c$ . In case of events with more than  
 110 two such leptons, we select the pair that maximizes the scalar sum of lepton  $p_T$ 's. Events with  $ee/\mu\mu$   
 111 dilepton mass consistent with  $Z \rightarrow ee/\mu\mu$  are rejected, and the mass “window” for which we apply this  
 112 veto is defined from 76 GeV/ $c^2$  to 106 GeV/ $c^2$ . We also remove events with dilepton invariant mass  $<$   
 113 12 GeV/ $c^2$  to remove events with Upsilon's. There must be at least two pfjets of  $p_T > 30$  GeV/ $c$  and  
 114  $|\eta| < 2.5$  and at least one of them must pass the CSVM b-tagging requirement [15]; jets must pass loose  
 115 pfJetId, and be separated by  $\Delta R > 0.4$  from any lepton passing the selection. We require  $E_T^{\text{miss}} > 30$   
 116 GeV, using pfmet. More details are given in the subsections below.

#### 117 3.1 Event Cleanup

- 118 • Require at least one good deterministic annealing (DA) vertex
- 119     – not fake
- 120     – ndof  $> 4$
- 121     –  $|\rho| < 2$  cm
- 122     –  $|z| < 24$  cm.

#### 123 3.2 Muon Selection

124 Muon candidates are RECO muon objects passing the following requirements:

- 125 •  $p_T > 20$  GeV and  $|\eta| < 2.4$
- 126 • Global Muon and Tracker Muon
- 127 •  $\chi^2/\text{ndof}$  of global fit  $< 10$
- 128 • At least 11 hits in the tracker fit
- 129 • Impact parameter with respect to the first good DA vertex  $d_0 < 200$   $\mu\text{m}$  and  $d_z < 1$  cm
- 130 • iso  $\equiv E_T^{\text{iso}}/p_T < 0.15$ ,  $E_T^{\text{iso}}$  is defined as the sum of transverse energy/momentum deposits in ecal,  
 131 hcal, and tracker, in a cone of 0.3
- 132 • At least one of the hits from the standalone muon must be used in the global fit
- 133 • Tracker  $\Delta p_T/p_T < 0.1$

### 3.3 Electron Selection

Electron candidates are RECO GSF electrons passing the following requirements:

- $p_T > 20$  GeV and  $|\eta| < 2.5$ .
- Veto electrons with a supercluster in the transition region  $1.4442 < |\eta| < 1.556$ .
- VBTF90 identification[17] with requirements tightened to match the CaloIdT and TrkIdVL HLT requirements:
  - $\sigma_{i\eta i\eta} < 0.01$  (EB), 0.03 (EE)
  - $\Delta\phi < 0.15$  (EB), 0.10 (EE)
  - $\Delta\eta < 0.007$  (EB), 0.009 (EE)
  - $H/E < 0.1$  (EB), 0.075 (EE)
- Impact parameter with respect to the first good DA vertex  $d_0 < 400$   $\mu\text{m}$  and  $d_z < 1$  cm.
- $\text{iso} \equiv E_T^{\text{iso}}/p_T < 0.15$ .  $E_T^{\text{iso}}$  is defined as the sum of transverse energy/momentum deposits in ecal, hcal, and tracker, in a cone of 0.3. A 1 GeV pedestal is subtracted from the ecal energy deposition in the EB, however the ecal energy is never allowed to go negative.
- Electrons with a tracker or global muon within  $\Delta R$  of 0.1 are vetoed.
- The number of missing expected inner hits must be less than two [18].
- Conversion removal via partner track finding: any electron where an additional GeneralTrack is found with  $|dist| < 0.02$  cm and  $|\Delta \cot \theta| < 0.02$  is vetoed [18].

We estimate the contributions from fake leptons using the data-driven fake rate (FR) method in Section 8. The requirements defining the fakeable objects are listed in App. A.

### 3.4 Trigger Selection

We do not make any requirements on HLT bits in the Monte Carlo. Instead, as discussed in Section 4, a trigger efficiency weight is applied to each event, based on the trigger efficiencies measured on data (see Section 4).

We select data events using the following triggers. An event in the  $ee$  channel is required to pass a DoubleElectron trigger, an event in the  $\mu\mu$  channel is required to pass a DoubleMu trigger, and an event in the  $e\mu$  channel is required to pass a Ele-Mu trigger.

- Double Electron
  - HLT\_Ele17\_CaloIdL\_CaloIsoVL\_Ele8\_CaloIdL\_CaloIsoVL
  - HLT\_Ele17\_CaloIdT\_TrkIdVL\_CaloIsoVL\_TrkIsoVL\_Ele8\_CaloIdT\_TrkIdVL\_CaloIsoVL\_TrkIsoVL
  - HLT\_Ele17\_CaloIdT\_CaloIsoVL\_TrkIdVL\_TrkIsoVL\_Ele8\_CaloIdT\_CaloIsoVL\_TrkIdVL\_TrkIsoVL
- Double Muon
  - HLT\_DoubleMu7
  - HLT\_Mu13\_Mu7
  - HLT\_Mu13\_Mu8
  - HLT\_Mu17\_Mu8
- Electron Muon
  - HLT\_Mu17\_Ele8\_CaloIdL
  - HLT\_Mu8\_Ele17\_CaloIdL
  - HLT\_Mu17\_Ele8\_CaloIdT\_CaloIsoVL
  - HLT\_Mu8\_Ele17\_CaloIdT\_CaloIsoVL

## 175 4 Trigger efficiency

176 For the high  $p_T$  dilepton triggers, the efficiencies listed in Table 1, Table 2, Table 3 and Table 4 are  
 177 applied to  $ee$ ,  $\mu\mu$  and  $e\mu$  Monte Carlo Events. Details of the measurement of the trigger efficiencies are  
 178 described in [16].

Table 1: The efficiency of the leading leg requirement for the double electron trigger, averaged over the full 2011 data.

Measurement	$0.0 \leq  \eta  < 1.5$	$1.5 \leq  \eta  < 2.5$
$20 \leq p_T \leq 30$	$0.9849 \pm 0.0003$	$0.9774 \pm 0.0007$
$p_T > 30$	$0.9928 \pm 0.0001$	$0.9938 \pm 0.0001$

Table 2: The efficiency of the trailing leg requirement for the double electron trigger, averaged over the full 2011 data.

Measurement	$0.0 \leq  \eta  < 1.5$	$1.5 \leq  \eta  < 2.5$
$20 \leq p_T \leq 30$	$0.9923 \pm 0.0002$	$0.9953 \pm 0.0003$
$p_T > 30$	$0.9948 \pm 0.0001$	$0.9956 \pm 0.0001$

Table 3: The efficiency of the leading leg requirement for the double muon trigger, averaged over the full 2011 data.

Measurement	$0.0 \leq  \eta  < 0.8$	$0.8 \leq  \eta  < 1.2$	$1.2 \leq  \eta  < 2.1$	$2.1 \leq  \eta  < 2.4$
$20 \leq p_T \leq 30$	$0.9648 \pm 0.0007$	$0.9516 \pm 0.0013$	$0.9480 \pm 0.0009$	$0.8757 \pm 0.0026$
$p_T > 30$	$0.9666 \pm 0.0003$	$0.9521 \pm 0.0005$	$0.9485 \pm 0.0004$	$0.8772 \pm 0.0012$

Table 4: The efficiency of the trailing leg requirement for the double muon trigger, averaged over the full 2011 data.

Measurement	$0.0 \leq  \eta  < 0.8$	$0.8 \leq  \eta  < 1.2$	$1.2 \leq  \eta  < 2.1$	$2.1 \leq  \eta  < 2.4$
$20 \leq p_T \leq 30$	$0.9655 \pm 0.0007$	$0.9535 \pm 0.0013$	$0.9558 \pm 0.0009$	$0.9031 \pm 0.0023$
$p_T > 30$	$0.9670 \pm 0.0003$	$0.9537 \pm 0.0005$	$0.9530 \pm 0.0004$	$0.8992 \pm 0.0011$

## 179 5 $b$ -tagging Scale Factor

180  $b$ -tagging scale factors are applied to MC events for each jet, due to the difference of  $b$ -tagging efficiencies  
 181 between data and MC [15]. The scale factor for  $b$ -tagging efficiency (CSVM) is 0.97 [15].

## 182 6 Observables

183 The definitions of the observables are the following:

- Lepton charge asymmetry:

$$A_{lepC} = \frac{N(|\eta_+| > |\eta_-|) - N(|\eta_+| < |\eta_-|)}{N(|\eta_+| > |\eta_-|) + N(|\eta_+| < |\eta_-|)}$$

184 where  $|\eta_l|$  is the Rapidity (Pseudo-rapidity) of leptons.

- Lepton azimuthal angle asymmetry:

$$A_{lepAzim} = \frac{N(\cos\Delta\phi_{l+l-} > 0) - N(\cos\Delta\phi_{l+l-} < 0)}{N(\cos\Delta\phi_{l+l-} > 0) + N(\cos\Delta\phi_{l+l-} < 0)}$$

185 where  $\Delta\phi$  is the azimuthal angle between the two leptons.

- Top charge asymmetry:

$$A_{topC} = \frac{N(\cos(\theta_t) > 0) - N(\cos(\theta_t) < 0)}{N(\cos(\theta_t) > 0) + N(\cos(\theta_t) < 0)}$$

186 where  $\theta_t$  is the production angle of the top quark in the  $t\bar{t}$  rest frame with respect to the direction  
187 of the boost of the  $t\bar{t}$  system.

- Top polarization:

$$P_n = \frac{N(\cos(\theta_l^+) > 0) - N(\cos(\theta_l^+) < 0)}{N(\cos(\theta_l^+) > 0) + N(\cos(\theta_l^+) < 0)}$$

188 where  $\theta_l^+$  is the production angle of the positively charged lepton in the rest frame of its parent  
189 top, with respect to the direction of the parent top in the  $t\bar{t}$  rest frame.

- Top spin correlation:

$$A_{topSpinCorrelation} = \frac{N(\cos(\theta_l^+) * \cos(\theta_l^-) > 0) - N(\cos(\theta_l^+) * \cos(\theta_l^-) < 0)}{N(\cos(\theta_l^+) * \cos(\theta_l^-) > 0) + N(\cos(\theta_l^+) * \cos(\theta_l^-) < 0)}$$

190 where  $\theta_l^-$  is the production angle of the negatively charged lepton in the rest frame of its parent  
191 anti-top, with respect to the direction of the parent anti-top in the  $t\bar{t}$  rest frame.

## 192 7 Preselection yields: Data/MC Comparison

193 The data yields and the MC predictions for the preselection are given in Table 5. The MC predicts that  
194 the preselection is dominated by  $t\bar{t} \rightarrow \ell^+\ell^-$  (92%), with the largest background coming from single top  
195 production. The MC yields are normalized to  $5.0 \text{ fb}^{-1}$  using the cross sections from Section 2. The  $t\bar{t}$   
196 yields are normalized such that the total MC yield matches the data. The MC events have been weighted  
197 such that the distribution of reconstructed DA vertices matches that in data.

Table 5: The observed and expected yields after the preselection described in the text, for an integrated luminosity of  $5.0 \text{ fb}^{-1}$ . Uncertainties are statistical only. Upper limits are given where yields are zero due to statistical limitations of the simulated event samples.

Sample	ee	$\mu\mu$	$e\mu$	all
$t\bar{t} \rightarrow \ell^+\ell^-$	$1791.7 \pm 4.4$	$2127.3 \pm 4.7$	$5069.4 \pm 7.3$	$8988.5 \pm 9.7$
$t\bar{t} \rightarrow \text{fake}$	$32.5 \pm 2.9$	$4.8 \pm 1.1$	$53.3 \pm 3.6$	$90.7 \pm 4.8$
$W + \text{jets}$	$< 1.9$	$4.7 \pm 3.3$	$4.7 \pm 3.4$	$9.4 \pm 4.7$
$DY \rightarrow ee$	$52.3 \pm 5.8$	$< 0.6$	$< 0.6$	$52.3 \pm 5.8$
$DY \rightarrow \mu\mu$	$< 0.6$	$72.8 \pm 6.5$	$1.6 \pm 0.9$	$74.4 \pm 6.5$
$DY \rightarrow \tau\tau$	$17.6 \pm 3.3$	$8.7 \pm 2.2$	$18.7 \pm 3.2$	$45.0 \pm 5.1$
Di-boson	$10.6 \pm 0.5$	$13.0 \pm 0.5$	$24.0 \pm 0.7$	$47.6 \pm 1.0$
Single top	$84.9 \pm 2.3$	$101.2 \pm 2.4$	$252.1 \pm 3.9$	$438.2 \pm 5.1$
Total Background	$1989.6 \pm 8.8$	$2332.6 \pm 9.3$	$5423.8 \pm 10.3$	$9746.0 \pm 16.4$
Data	1961	2373	5412	9746

198 Data and MC comparison plots for the number of b tagged jets and the number of vertices are shown in  
199 Figure 1, and more comparison plots for the preselection region can be found in App. B.

200 A comparison between data and MC for the five asymmetry variables is given in Figures 2, 3 and 4.  
201 Each plot shows the MC distributions when using the three different  $t\bar{t}$  samples of Section 2 for the

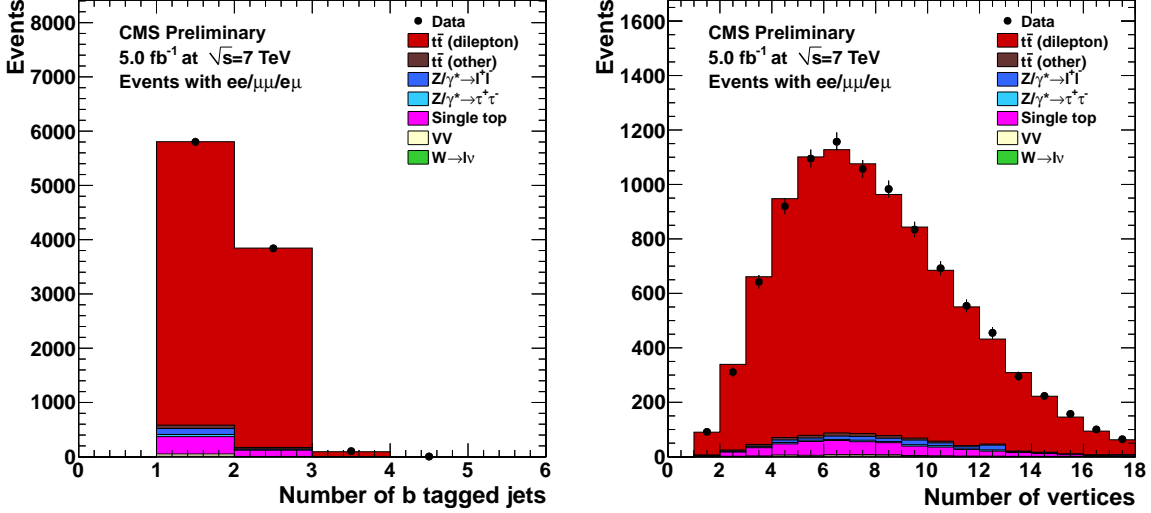


Figure 1: Comparison of data and MC for number of b tagged jets (left) and number of vertices (right). More comparison plots can be found in App. B.

202  $t\bar{t} \rightarrow \ell^+\ell^-$  component, with the background components of Table 5 used in each case. All distributions  
 203 are normalized to unity, and K-S values are given (calculated using 5 times finer binning than is plotted).  
 204 The powheg-pythia sample best represents the data in the preselection region, and is thus chosen as the  
 205 default sample for the analysis.

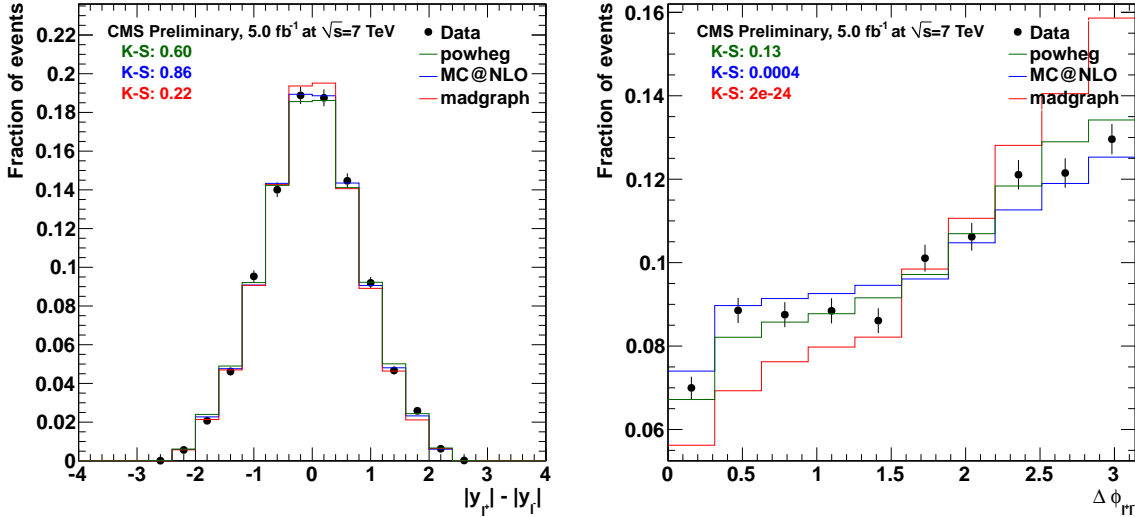


Figure 2: Comparison between data and the three different  $t\bar{t}$  MC samples in the preselection region for lepton charge asymmetry (left) and lepton azimuthal asymmetry (right). The MC background of Table 5 is added to each of the  $t\bar{t}$  samples, and all distributions are normalized to unity.

## 206 8 Background Estimation

207 We use data driven methods to cross-check the MC estimates for the background contributions from  
 208 events with fake leptons and from  $DY \rightarrow ee/\mu\mu$  events. We rely on MC alone to predict the remaining  
 209 events, which are dominated by  $tW$  production. Predictions are made for the preselection region and for  
 210 the two signal regions (Section 9):

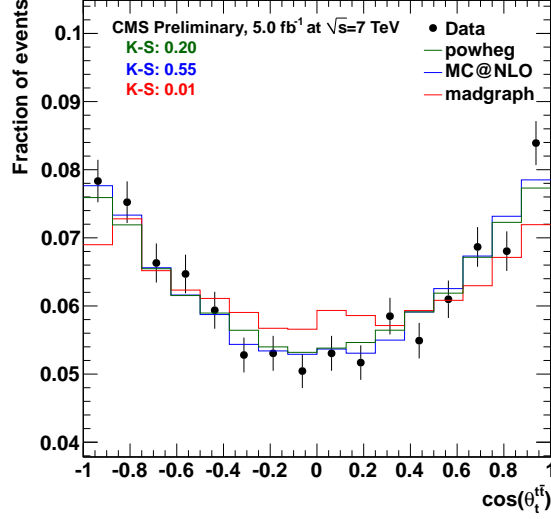


Figure 3: Comparison between data and the three different  $t\bar{t}$  MC samples in the preselection region for top charge asymmetry. The MC background of Table 5 is added to each of the  $t\bar{t}$  samples, and all distributions are normalized to unity. Since this variable requires  $t\bar{t}$  reconstruction, only those events with a top solution are plotted.

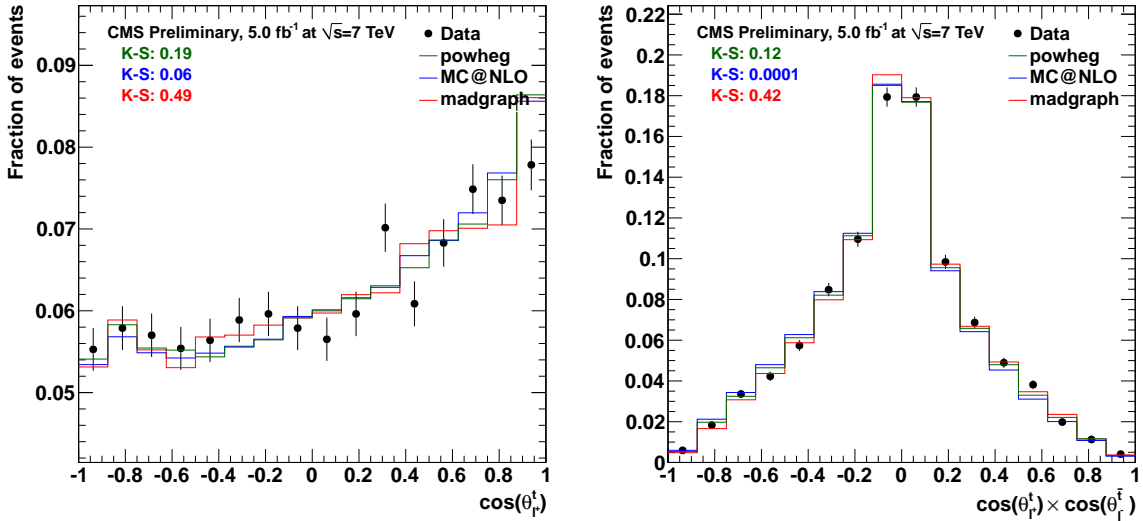


Figure 4: Comparison between data and the three different  $t\bar{t}$  MC samples in the preselection region for top polarization (left) and top spin correlation (right). The MC background of Table 5 is added to each of the  $t\bar{t}$  samples, and all distributions are normalized to unity. Since these variables require  $t\bar{t}$  reconstruction, only those events with a top solution are plotted.

- 211 • Signal Region *I*:  $M_{t\bar{t}} > 450 \text{ GeV}/c^2$
- 212 • Signal Region *II*:  $M_{t\bar{t}} > 450 \text{ GeV}/c^2$  and  $|y_t + y_{\bar{t}}| > 2.0$ .

213 The data-driven lepton tight-to-loose method for estimating the events with fake leptons is described in  
 214 Section 8.1, and the data-driven  $R_{out/in}$  method to estimate the Drell-Yan background is described in  
 215 Section 8.2.

## 216 8.1 Fake lepton background estimation

217 We use the “tight-to-loose” method [22] to predict the number of events with one fake lepton. We select  
 218 events where one of the leptons passes the full selection and the other one fails the full selection but  
 219 passes the “Fakeable Object” selection of Reference [22] (see also App. A). We then weight each event  
 220 by  $FR/(1-FR)$  where  $FR$  is the “fake rate” for the fakeable object.

221 We apply this method to events passing the other selection requirements in data. In the preselection  
 222 region, the raw result is  $560 \pm 16 \pm 280$ , where the first uncertainty is statistical and the second uncertainty  
 223 is from the 50% systematic uncertainty associated with this method [22]. The raw result has to be  
 224 corrected for “signal contamination”, *i.e.*, the contribution from true dilepton events with one lepton  
 225 failing the selection. This is estimated from Monte Carlo to be  $415 \pm 7$ , where the uncertainty is from  
 226 MC statistics only. Thus, the estimated number of events with one “fake” lepton is  $145_{-145}^{+280}$ .

227 We can also apply a similar technique to estimate backgrounds with two fake leptons, *e.g.*, from QCD  
 228 events. In this case we select events with both leptons failing the full selection but passing the “Fakeable  
 229 Object” selection. The resulting prediction in data is  $10_{-10}^{+19}$  events. This contribution is double-counted  
 230 in the prediction for one fake lepton, and is thus subtracted from the total to give a final estimate of  
 231  $134_{-134}^{+281}$  events with fake leptons. The Monte Carlo expectation for this contribution can be obtained by  
 232 summing up the  $t\bar{t} \rightarrow \text{fake}$  and  $W + \text{jets}$  entries from Table 5. This result is  $100.1 \pm 6.7$  (stat. error  
 233 only), consistent with the data-driven prediction.

234 In Signal Region *I*, the raw result for the contribution with one fake lepton is  $216.2 \pm 9.7 \pm 108.5$ , from  
 235 which  $175.5 \pm 4.5$  is subtracted to account for signal contamination (estimated from MC) to give an  
 236 estimate of  $40.7_{-40.7}^{+108.6}$ . The prediction for the contribution from events with two fake leptons is  $4.2_{-4.2}^{+7.3}$   
 237 events, which is subtracted from the prediction for one fake lepton to give a final estimate of  $36.5_{-36.4}^{+108.9}$   
 238 events with fake leptons. The Monte Carlo expectation for this contribution (Table 10) is  $46.8 \pm 5.4$ ,  
 239 consistent with the data-driven prediction.

## 240 8.2 Drell-Yan background estimation

241 The method is based on counting the number of  $Z$  candidates<sup>1)</sup> passing the selection with reversed  $Z$  veto,  
 242 subtracting the number of non Drell-Yan events estimated using the number of  $e\mu$  events, then scaling  
 243 by the expected ratio of Drell-Yan events outside/inside the  $Z$  mass window. This ratio is called  $R_{out/in}$   
 244 and is obtained from Monte Carlo.

245 The results for the preselection region are summarized in Table 6, giving an estimate of  $142.5 \pm 11.6$  Drell-  
 246 Yan events ( $ee + \mu\mu$ ) in the preselection region. The result is thus consistent with the MC prediction of  
 247  $126.5 \pm 8.7$  from Table 5. We also perform a closure test of the method using MC, and the results are  
 248 summarized in Table 7.

249 The results for Signal Region *I* are summarized in Table 8, giving an estimate of  $47.6 \pm 6.7$  Drell-Yan  
 250 events ( $ee + \mu\mu$ ) in the signal region. The result is thus consistent with the MC prediction of  $39.3 \pm 4.8$ .  
 251 We also perform a closure test of the method using MC, and the results are summarized in Table 9.

## 252 8.3 Remaining backgrounds

253 We rely on MC to predict the remaining backgrounds. The results are taken from Tables 5 and 10.

---

<sup>1)</sup>  $e^+e^-$  and  $\mu^+\mu^-$  with invariant mass inside the  $Z$  mass window.

Table 6: Data-driven Drell-Yan estimation in the preselection region.  $N_{in}$  is the number of events inside the Z window. Before subtraction from  $N_{in}$  for  $ee$  and  $\mu\mu$  data,  $N_{in}$  in  $e\mu$  data is multiplied by  $k/2$ , where  $k$  accounts for the difference in efficiencies for  $e$  and  $\mu$  and the factor of  $1/2$  is due to combinatorics.

Sample	ee	$\mu\mu$
$N_{in}$ in data	$1361.00 \pm 36.89$	$1575.00 \pm 39.69$
$N_{in}$ in $e\mu$ data	$1218.00 \pm 34.90$	
$k$	$0.93 \pm 0.02$	$1.08 \pm 0.02$
$R_{out/in}$	$0.07 \pm 0.01$	$0.09 \pm 0.01$
DY prediction (preselection)	$57.55 \pm 7.24$	$84.92 \pm 8.97$

Table 7: Closure test for data-driven Drell-Yan estimation in the preselection region. The calculation is the same as in Table 6, but with all data yields replaced by MC. The prediction of the method is consistent with the MC DY yields (bottom row).

Sample	ee	$\mu\mu$
$N_{in}$ in pseudodata	$1340.29 \pm 25.21$	$1488.01 \pm 25.52$
$N_{in}$ in $e\mu$ pseudodata	$1268.44 \pm 17.69$	
$k$	$0.95 \pm 0.01$	$1.05 \pm 0.01$
$R_{out/in}$	$0.07 \pm 0.01$	$0.09 \pm 0.01$
DY prediction (preselection)	$53.46 \pm 6.43$	$75.67 \pm 7.53$
DY MC event count	$52.24 \pm 5.76$	$72.74 \pm 6.47$

## 9 Signal region

254

255 After preselection, our sample is dominated by SM  $t\bar{t}$  events. To distinguish the signal events from the  
 256 background, we look at additional variables: the invariant mass of  $t\bar{t}$  ( $M_{t\bar{t}}$ ) and the absolute value of the  
 257 sum of the rapidities of top and anti-top ( $|y_t + y_{\bar{t}}|$ ).

258 The two signal regions are chosen on top of the preselection:

- 259 • Signal Region I:  $M_{t\bar{t}} > 450 \text{ GeV}/c^2$
- 260 • Signal Region II:  $M_{t\bar{t}} > 450 \text{ GeV}/c^2$  and  $|y_t + y_{\bar{t}}| > 2.0$

261 These two regions are interesting because the new physics enters in the high  $M_{t\bar{t}}$  region and the  $t\bar{t}$   
 262 production from gluon-gluon fusion is significantly suppressed in the forward region.

### 9.1 Signal region I

263

264 Data yields and MC expectations in the signal region I are shown in Table 10. Reasonable agreement  
 265 between data and MC expectations is observed. The reconstructed asymmetries are listed in Table 11.  
 266 A comparison of data and MC is shown in Figures 5, 6 and 7.

Table 8: Data-driven Drell-Yan estimation in the signal region.  $N_{in}$  is the number of events inside the Z window. Before subtraction from  $N_{in}$  for  $ee$  and  $\mu\mu$  data,  $N_{in}$  in  $e\mu$  data is multiplied by  $k/2$ , where  $k$  accounts for the difference in efficiencies for  $e$  and  $\mu$  and the factor of  $1/2$  is due to combinatorics.

Sample	ee	$\mu\mu$
$N_{in}$ in data	$516.00 \pm 22.72$	$603.00 \pm 24.56$
$N_{in}$ in $e\mu$ data	$441.00 \pm 21.00$	
$k$	$0.93 \pm 0.03$	$1.08 \pm 0.03$
$R_{out/in}$	$0.06 \pm 0.01$	$0.08 \pm 0.01$
DY prediction (signal region)	$17.30 \pm 3.98$	$30.33 \pm 5.30$

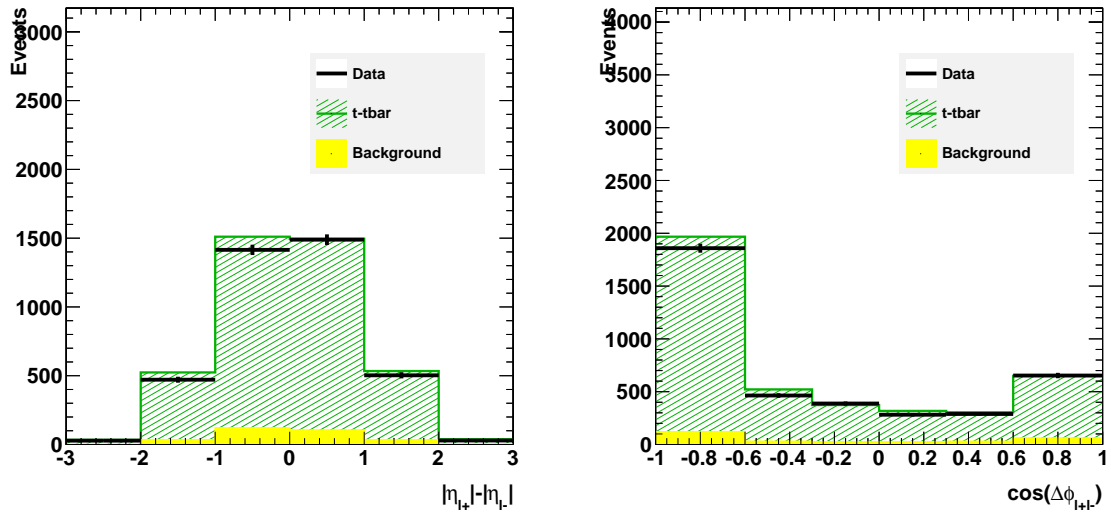


Figure 5: Comparison between data and MC samples in the signal region  $I$  for lepton charge asymmetry (left) and lepton azimuthal asymmetry (right).

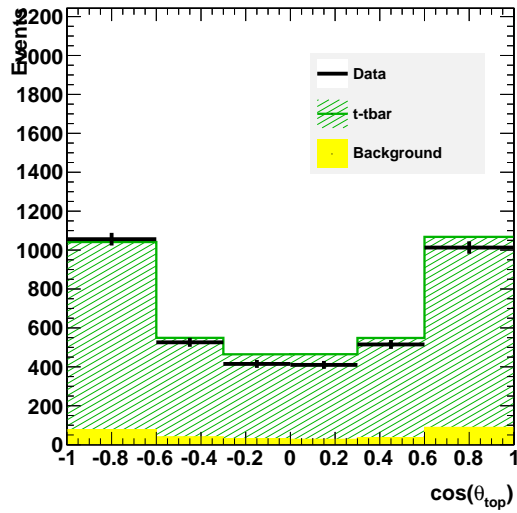


Figure 6: Comparison between data and the MC samples in the signal region  $I$  for top charge asymmetry.

Table 9: Closure test for data-driven Drell-Yan estimation in the signal region. The calculation is the same as in Table 8, but with all data yields replaced by MC. The prediction of the method is consistent with the MC DY yields (bottom row).

Sample	ee	$\mu\mu$
$N_{in}$ in pseudodata	$476.41 \pm 14.79$	$564.75 \pm 15.74$
$N_{in}$ in $e\mu$ pseudodata	$468.86 \pm 10.83$	
$k$	$0.92 \pm 0.02$	$1.09 \pm 0.02$
$R_{out/in}$	$0.06 \pm 0.01$	$0.08 \pm 0.01$
DY prediction (signal region)	$14.48 \pm 3.24$	$25.75 \pm 4.30$
DY MC event count	$13.83 \pm 2.89$	$25.49 \pm 3.83$

Table 10: The observed and expected yields in the signal region  $I$  for  $5.0 \text{ fb}^{-1}$ . Uncertainties are statistical only. Some of the expected yields are zero due to statistical limitations of the simulated event samples.

Sample	ee	$\mu\mu$	$e\mu$	all
$t\bar{t} \rightarrow \ell^+\ell^-$	$774.3 \pm 14.3$	$896.9 \pm 14.9$	$2136.7 \pm 23.4$	$3807.9 \pm 31.2$
$t\bar{t} \rightarrow \text{fake}$	$14.5 \pm 1.9$	$1.5 \pm 0.6$	$23.3 \pm 2.4$	$39.3 \pm 3.1$
$W + \text{jets}$	$0.0 \pm 0.0$	$4.7 \pm 3.3$	$2.8 \pm 2.8$	$7.5 \pm 4.4$
DY $\rightarrow \ell^+\ell^-$	$21.3 \pm 3.6$	$28.1 \pm 4.0$	$8.5 \pm 2.2$	$57.9 \pm 5.8$
Di-boson	$3.9 \pm 0.3$	$4.7 \pm 0.3$	$9.7 \pm 0.5$	$18.3 \pm 0.6$
Single top	$32.7 \pm 1.4$	$41.7 \pm 1.5$	$100.9 \pm 2.5$	$175.2 \pm 3.2$
Total Background	$846.7 \pm 15.0$	$977.6 \pm 15.8$	$2281.9 \pm 23.9$	$4106.2 \pm 32.4$
Data	$801.0 \pm 28.3$	$970.0 \pm 31.1$	$2164.0 \pm 46.5$	$3935.0 \pm 62.7$

Table 11: Reconstructed asymmetries in the signal region  $I$ .

Reconstructed asymmetries	MC	Data
Lepton charge	$0.000 \pm 0.003$	$0.027 \pm 0.016$
Lepton azimuthal angle	$-0.384 \pm 0.003$	$-0.378 \pm 0.019$
Top charge	$0.006 \pm 0.003$	$-0.015 \pm 0.016$
Top polarization	$0.106 \pm 0.003$	$0.101 \pm 0.016$
Top spin correlation	$-0.044 \pm 0.003$	$-0.019 \pm 0.016$

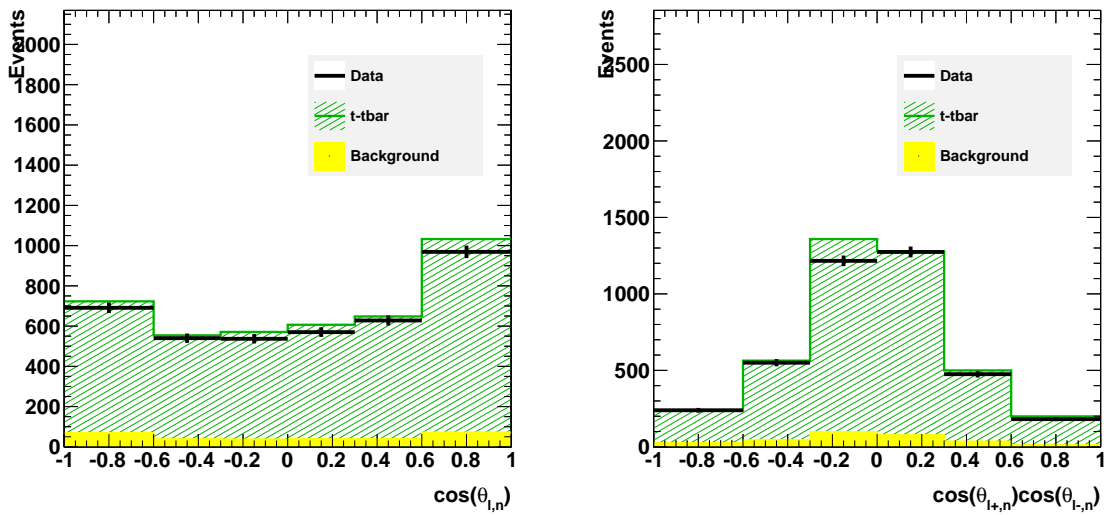


Figure 7: Comparison between data and the MC samples in the signal region  $I$  for top polarization (left) and top spin correlation (right).

267 **9.2 Signal region II**

268 Data yields and MC expectations in the signal region II are shown in Table 12. Reasonable agreement  
 269 between data and MC expectations is observed. The reconstructed asymmetries are listed in Table 13.  
 270 A comparison of data and MC is shown in Figures 8, 9 and 10. .

Table 12: The observed and expected yields in the signal region II for  $5.0 \text{ fb}^{-1}$ . Uncertainties are statistical only. Some of the expected yields are zero due to statistical limitations of the simulated event samples.

Sample	ee	$\mu\mu$	$e\mu$	all
$t\bar{t} \rightarrow \ell^+\ell^-$	$103.3 \pm 5.3$	$115.2 \pm 5.3$	$285.8 \pm 8.6$	$504.3 \pm 11.4$
$t\bar{t} \rightarrow \text{fake}$	$2.7 \pm 0.9$	$0.4 \pm 0.3$	$2.8 \pm 0.8$	$6.0 \pm 1.2$
$W + \text{jets}$	$0.0 \pm 0.0$	$2.2 \pm 2.2$	$0.0 \pm 0.0$	$2.2 \pm 2.2$
$\text{DY} \rightarrow \ell^+\ell^-$	$2.5 \pm 1.3$	$7.4 \pm 2.1$	$1.4 \pm 0.8$	$11.4 \pm 2.6$
Di-boson	$0.6 \pm 0.1$	$0.5 \pm 0.1$	$1.4 \pm 0.2$	$2.5 \pm 0.2$
Single top	$3.6 \pm 0.5$	$5.9 \pm 0.6$	$13.3 \pm 0.9$	$22.9 \pm 1.2$
Total Background	$112.8 \pm 5.5$	$131.7 \pm 6.1$	$304.7 \pm 8.7$	$549.3 \pm 12.0$
Data	$103.0 \pm 10.1$	$116.0 \pm 10.8$	$258.0 \pm 16.1$	$477.0 \pm 21.8$

Table 13: Reconstructed asymmetries in the signal region II.

Reconstructed asymmetries	MC	Data
Lepton charge	$0.002 \pm 0.008$	$-0.019 \pm 0.046$
Lepton azimuthal angle	$-0.441 \pm 0.010$	$-0.413 \pm 0.056$
Top charge	$0.007 \pm 0.008$	$0.031 \pm 0.046$
Top polarization	$0.069 \pm 0.008$	$-0.006 \pm 0.046$
Top spin correlation	$-0.017 \pm 0.008$	$0.006 \pm 0.046$

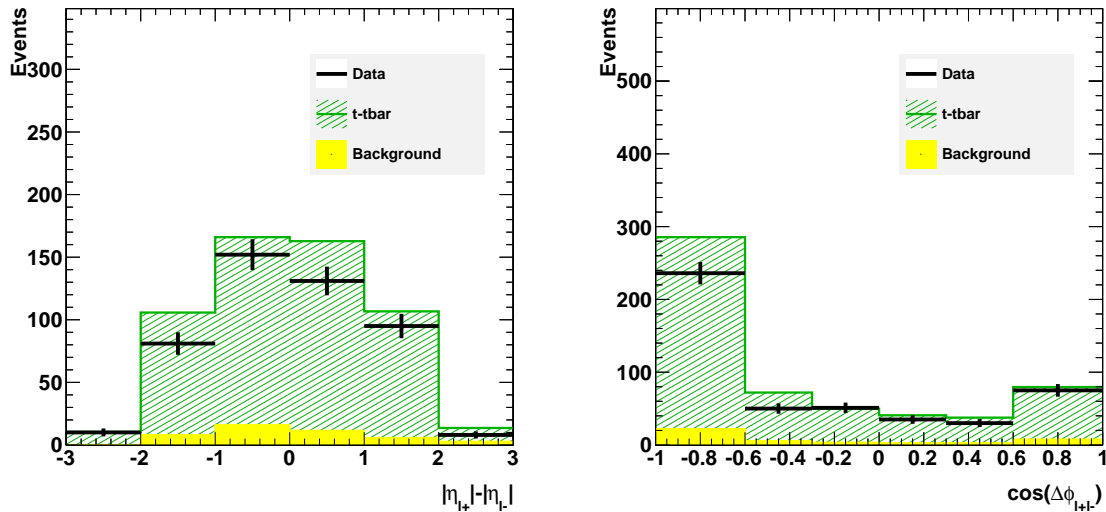


Figure 8: Comparison between data and MC samples in the signal II region for lepton charge asymmetry (left) and lepton azimuthal asymmetry (right).

271 **10 Unfolding**

272 The measured distributions are distorted from the true underlying distributions by the limited acceptance  
 273 of our detector and by bin-to-bin smearing due to a finite resolution of these variables. We have developed  
 274 a procedure that allows us to correct the binned data for both effects, yielding “parton-level” distributions

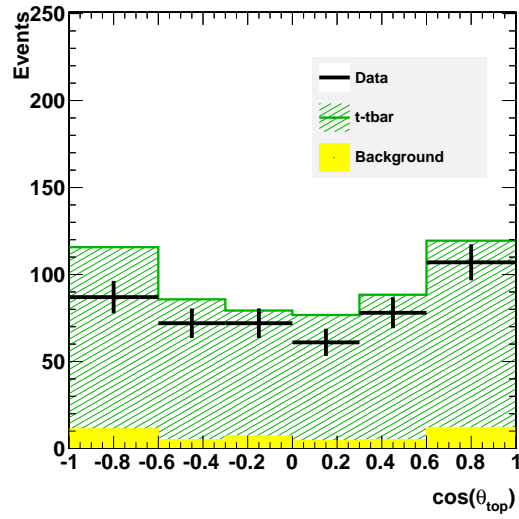


Figure 9: Comparison between data and the MC samples in the signal region *II* for top charge asymmetry.

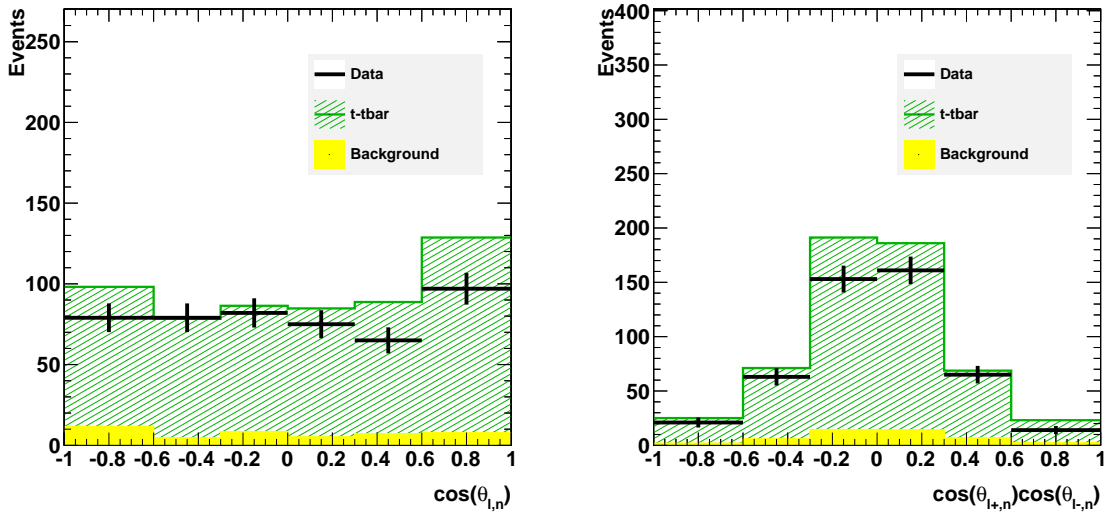


Figure 10: Comparison between data and the MC samples in the signal region *II* for top polarization (left) and top spin correlation (right).

275 and asymmetries. Our final results are normalized to the theoretical  $t\bar{t}$  cross-section of 154.0 pb, so that  
 276 the corrected distributions represent the differential cross-section in the variable of interest.

277 There are two effects that can alter the distributions of variables of interest. First, reconstruction and  
 278 identification requirements and the kinematic fitter are known to smear out the true kinematics of recon-  
 279 structed leptons and top quarks. In addition to reconstruction smearing effects, the true distributions  
 280 are also modified by event selection itself, which cuts out some  $t\bar{t}$  events. If the acceptance is biased with  
 281 respect to the asymmetry variable, such bias would cause a change in the asymmetry.

282 In general, after backgrounds are subtracted, the measured distribution  $\vec{b}$  is related to the underlying  
 283 parton-level distribution  $\vec{x}$  by the matrix equation:

$$\vec{b} = SA\vec{x},$$

284 where  $A$  is a diagonal matrix describing the acceptance in each bin of the measured distribution, while  
 285  $S$  is a non-diagonal smearing matrix describing the migration of events between bins due to the detector  
 286 resolution and reconstruction techniques.

The  $A$  and  $S$  matrices are modeled using the NLO POWHEG  $t\bar{t}$  sample. The binned data is multiplied  
 by the inverse matrices to recover the true parton-level distributions from the background subtracted  
 distributions in data:

$$\vec{x} = A^{-1}S^{-1}\vec{b}.$$

## 287 10.1 Binning

288 In order to apply matrix based corrections, it becomes necessary to choose a binning scheme for all  
 289 histograms and matrices. While using a larger number of bins allows precision in understanding of  
 290 smearing, the correction method is limited by statistics in the data. Using too-fine binning would result  
 291 in large bin-to-bin oscillations caused by statistical fluctuations. However, using very few bins is also  
 292 sub-optimal due to reduced information about the smearing. Using unfolding studies described later in  
 293 this section we find that for our level of statistics, the use of six bins in each of the distributions of interest  
 294 is optimal. Bin size is variable and is chosen so that the number of events in each bin of the distribution  
 295 is roughly the same. Summary of the binning is provided in Table 14.

Table 14: Binning used in the distributions of variables.

Variable	B1	B2	B3	B4	B5	B6
$A_{lepC}$	[-3.0,-2.0]	[-2.0,-1.0]	[-1.0,-0.0]	[0.0, 1.0]	[1.0, 2.0]	[2.0, 3.0]
$A_{\Delta\phi}$	[-1.0,-0.6]	[-0.6,-0.3]	[-0.3,-0.0]	[0.0, 0.3]	[0.3, 0.6]	[0.6, 1.0]
$A_{topFB}$	[-1.0,-0.6]	[-0.6,-0.3]	[-0.3,-0.0]	[0.0, 0.3]	[0.3, 0.6]	[0.6, 1.0]
$P_n$	[-1.0,-0.6]	[-0.6,-0.3]	[-0.3,-0.0]	[0.0, 0.3]	[0.3, 0.6]	[0.6, 1.0]
$A_{c1c2}$	[-1.0,-0.6]	[-0.6,-0.3]	[-0.3,-0.0]	[0.0, 0.3]	[0.3, 0.6]	[0.6, 1.0]

## 296 10.2 Acceptance Effects

297 The  $A$  matrix represents a standard bin-by-bin acceptance correction. To obtain it, we look at truth  
 298 information for Monte Carlo events and calculate the ratio of events passing the selection to the number  
 299 of generated events in bins of the asymmetry variables. Using these bin-by-bin ratios we construct  $A$   
 300 whose diagonal contains the ratio information. Acceptance matrices for each of the distributions of  
 301 interest are shown in Fig. 11.

## 302 10.3 Smearing Effects

303 Before applying the acceptance correction, we must first remove the resolution smearing from the distri-  
 304 bution.

305 Smearing effect can be seen in Figure 12 which shows 2D distributions of the asymmetry variables at  
 306 generator and reconstructed levels using  $t\bar{t}$  Monte Carlo events. The smearing effects are very small for

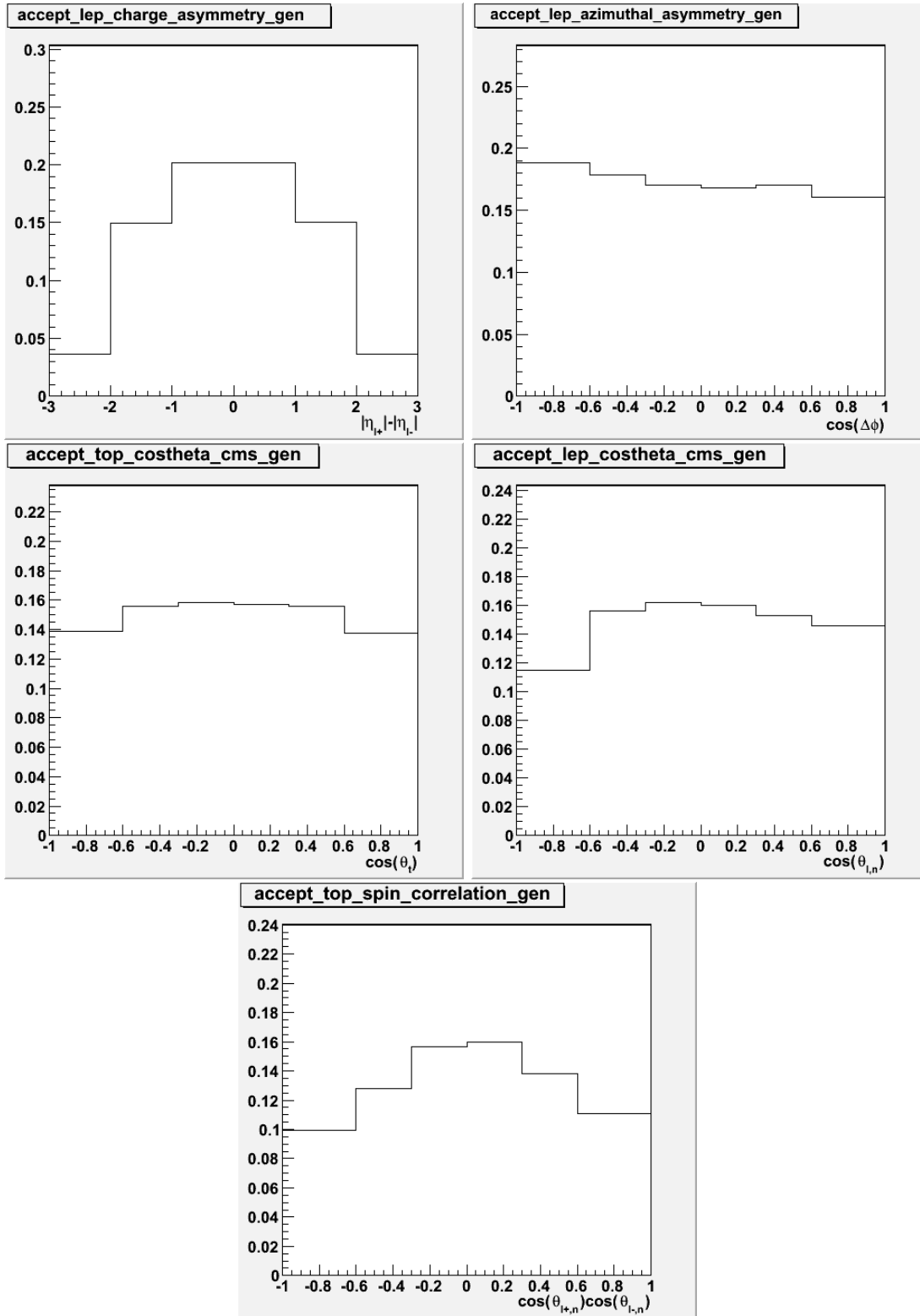


Figure 11: Acceptance matrix for each of the five measured variables.

307 the lepton-based observables, however for the ones requiring top reconstruction the effect is sizeable. Note  
 308 that most of the large values lie close to the diagonal, meaning there is little extreme smearing between  
 309 far-apart bins. Another feature of the histogram is that it is roughly symmetrical around the diagonal,  
 310 which indicates that the smearing does not cause an asymmetry in reconstructed data (if none existed  
 311 in the true distribution), but rather will dilute an existing asymmetry in the true distribution. In this  
 312 analysis we employ the unsmearing or “unfolding” algorithm based on singular value decomposition.

313 The SVD algorithm is powerful because the unfolding procedure is reduced to the inversion of a diagonal  
 314 matrix. Additionally, the equation can be reweighted such that the entries of the response matrix corre-  
 315 spond to actual Monte Carlo events, rather than the more conventionally used probabilities, eliminating  
 316 the possibility of bins with few generated Monte Carlo events receiving disproportionately large weights.  
 317 This reweighting is described in [?] and implemented in RooUnfold package. However, at this point, the  
 318 SVD algorithm still faces the same problem with large statistical fluctuations that is faced by pure matrix  
 319 inversion. In order to combat these dominant statistical fluctuations, we introduce a regularization term  
 320 to our unfold, as described in [?]. Regularization strength is defined by the parameter  $k$ . For very large  $k$   
 321 ( $k =$  number of bins in the distribution), SVD unfolding is equivalent to matrix inversion. For very small  
 322  $k$ , the regularization condition is strongly enforced (for example, for  $k = 0$ , the unfolded histogram is  
 323 equivalent to the distribution used to create the response matrix, regardless of the measured distribution  
 324 used as input). In this way, the regularization condition necessarily introduces a bias when we perform  
 325 an unfold. This bias is the cost of controlling the large statistical fluctuations that we would otherwise  
 326 face. The severity of the bias introduced is studied using pseudoexperiments, and will be discussed for  
 327 each variable that we use. In this analysis we use  $k = 3$ , which is half of the number of bins used for each  
 328 of the variables. The choice of  $k$  was motivated by the effort to maintain balance between the statistical  
 329 uncertainty of the method and the size of the introduced bias. This is a conservative choice leading to a  
 330 slightly larger statistical uncertainty compared to choosing a smaller  $k$  value, but also reduces the degree  
 331 to which the corrections tend to bias the result to the response model.

332 In the smearing correction, bin contents are moved from one bin to another (in order to correct for  
 333 the migrations produced by finite resolution in the variables of interest.) As a result of this, the final  
 334 uncertainties at the parton level are correlated across bins. The true uncertainties are described by  
 335 a covariance matrix, which includes not only diagonal entries corresponding to the square of the bin  
 336 errors, but also off-diagonal terms corresponding to the correlations between bins. Therefore, we use full  
 337 covariance matrices in determining the values of the asymmetries.

## 338 10.4 Linearity Tests

We verify that the unfolding procedure is able to correctly unfold distributions with different levels of  
 asymmetry. In order to do this, we re-weight generated  $t\bar{t}$  events according to the linear function of the  
 variable for which the asymmetry is measured. For example, in the case of di-lepton charge asymmetry,  
 the re-weighting function is:

$$weight = 1 + K(|\eta_+| - |\eta_-|).$$

339 The parameter  $K$  is varied between -0.5 and 0.5 in steps of 0.2. This variation introduces asymmetry of  
 340 up to 40% in the distributions of interest, which is by far more than what is expected in  $t\bar{t}$  events in the  
 341 SM, and also in the presence of new physics (such as for example  $W'$  and axigluon exchange models). For  
 342 each value of  $K$ , we then generate 2000 pseudo-experiments, in which number of events in each bin of the  
 343 distribution is fluctuated according to the Poisson statistics, and then the distribution is unfolded. The  
 344 average value of the asymmetry in 2000 pseudo-experiments is then compared to the original true-level  
 345 value. Figure 13 shows the mean values of the unfolded asymmetries as a function of the true values.  
 346 We find a linear behavior of this distribution, suggesting that non-SM asymmetry values will be also  
 347 measured correctly. The offsets and slopes obtained in the linear function fit are summarized in Table 15.

We also look at the distribution of the pulls in the sets of 2000 pseudo-experiments corresponding to  
 $K = 0.3$ . The pull is defined as:

$$Pull = \frac{(A_{true} - A_{unfolded})}{\sigma(A_{unfolded})}.$$

348 The distribution of pulls is fit to a gaussian function. We find a small bias leading to asymmetry changes  
 349 by up to 1% in some of the observables, and assign it as an additional systematic uncertainty associated  
 350 with the unfolding bias. The width of the gaussian function obtained in the fit is 0.9 for all five  
 351 observables, indicating that we slightly over-estimate the error.

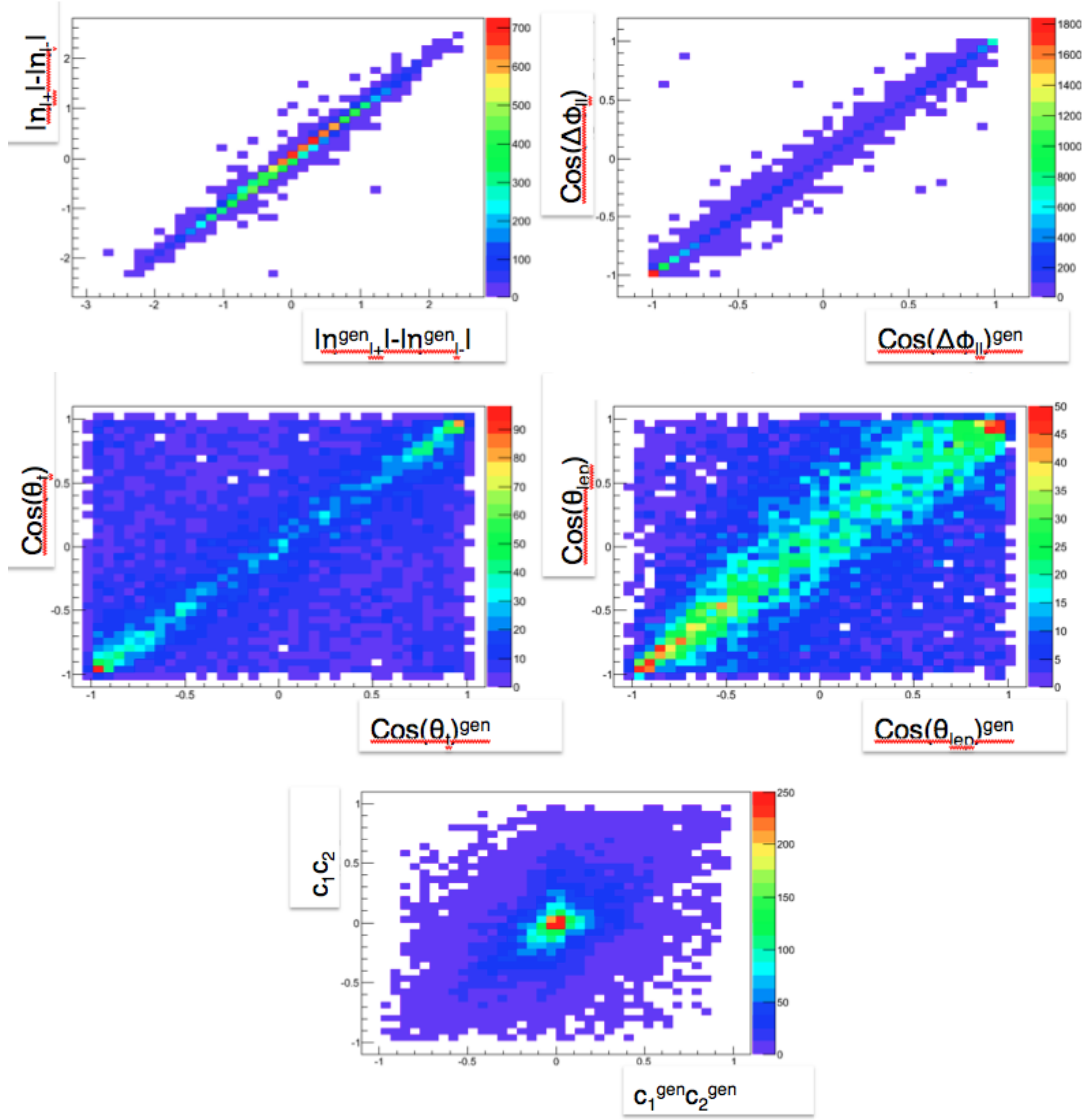


Figure 12: Smearing effects for each of the five measured variables.

Table 15: Summary of the linear function fit of the true vs unfolded asymmetry distribution.

Variable	offset	slope
$A_{lepC}$	$0.002 \pm 0.004$	$0.984 \pm 0.017$
$A_{\Delta\phi}$	$0.003 \pm 0.008$	$1.007 \pm 0.021$
$A_{topFB}$	$-0.004 \pm 0.011$	$1.027 \pm 0.061$
$P_n$	$-0.004 \pm 0.009$	$1.031 \pm 0.053$
$A_{c1c2}$	$0.009 \pm 0.012$	$1.121 \pm 0.164$

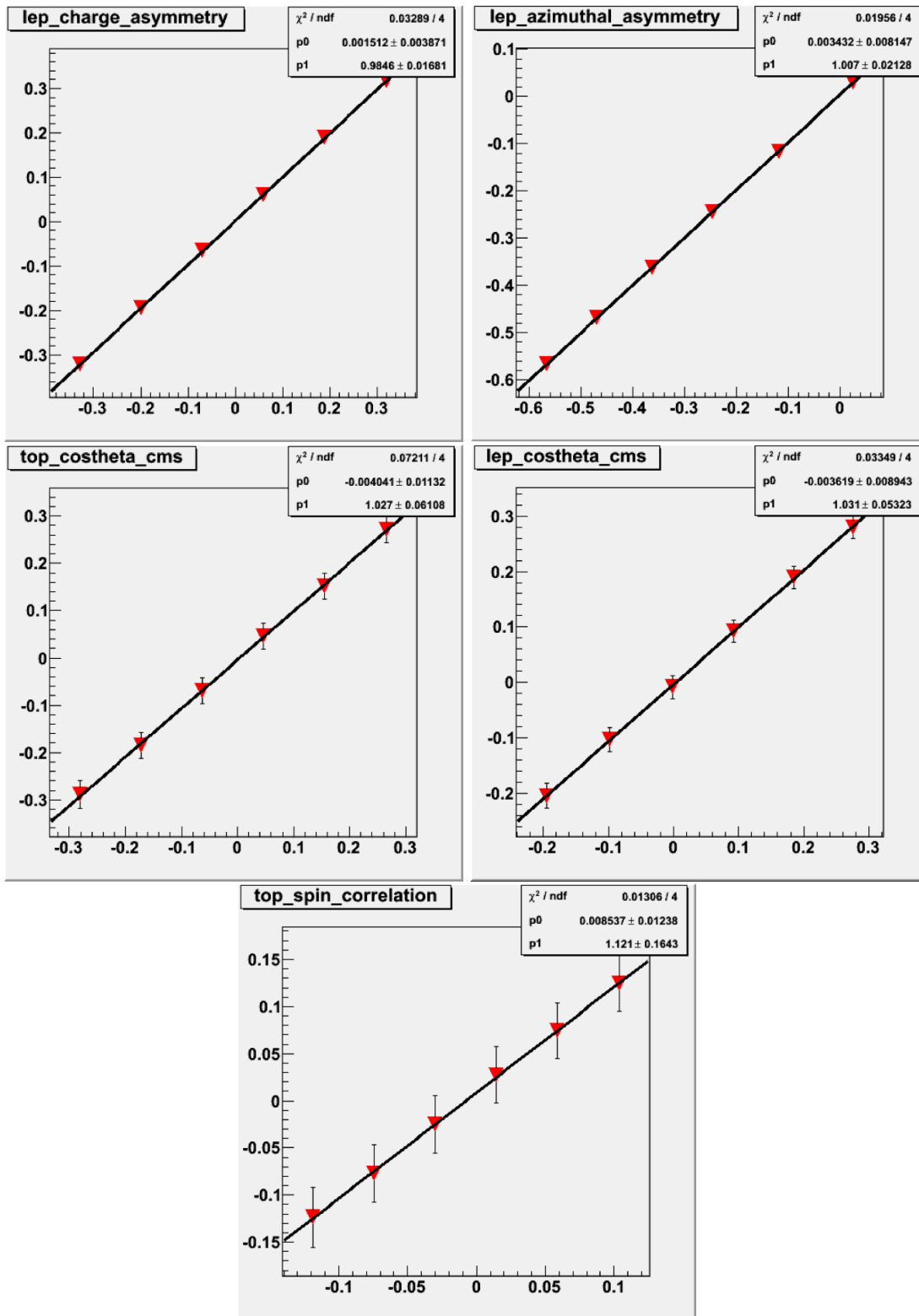


Figure 13: Linearity check of the unfolding procedure. X-axis corresponds to the true value of the asymmetry, while Y-axis corresponds to the unfolded one.

## 11 Systematics

One source of systematic uncertainty is associated with the jet and  $E_T^{\text{miss}}$  energy scale. We have used the method of Reference [14] to evaluate the systematic uncertainties due to the changes of the shape of the asymmetry distributions. The uncertainties are calculated assuming a 7.5% uncertainty to the hadronic energy scale in CMS, and are given in Table 16.

Table 16: Asymmetry variations due to the jet and  $E_T^{\text{miss}}$  energy scale in the preselection region.

Asymmetry variations	Scale up	Scale down
Lepton charge	0.003	0.001
Lepton azimuthal angle	0.01	0.02
Top charge	0.001	0.0
Top polarization	0.02	0.02
Top spin correlation	0.007	0.006

The second source of systematic uncertainty is associated with the background estimate. Given the uncertainties of the data driven background estimates described in Section 8, we increase DY and fake background by 100%. In addition, we increase the single top background by 50%. The uncertainties caused by the increasing of these background is described in Table 17.

Table 17: Asymmetry variations due to the background estimates in the preselection region.

Asymmetry variations	
Lepton charge	0.001
Lepton azimuthal angle	0.0
Top charge	0.001
Top polarization	0.007
Top spin correlation	0.003

The third source of systematic uncertainty is from the unfolding procedure. The systematic uncertainties due to the unfolding bias are given in Table 18. The systematics are small for the purely leptonic variables where the smearing is small.

Table 18: Asymmetry variations due to the unfolding

Asymmetry variations	
Lepton charge	0.001
Lepton azimuthal angle	0.002
Top charge	0.011
Top polarization	0.009
Top spin correlation	0.009

We also assess a systematic on  $t\bar{t}$  modeling by applying unfolding derived using MC@NLO  $t\bar{t}$  to powheg-pythia events, and taking the difference in result compared to that for the powheg-pythia derived unfolding. The results are summarized in Table 19. The resulting systematics are quite large for top polarization and top spin correlation, which we attribute to the difference in shape of the two MCs seen in Figure 4.

## 12 Results

Background-subtracted and unfolded asymmetry distributions based on the pre-selection region are shown in Figure 14. The measured asymmetry values (with statistical uncertainties only) are summarized in Table 20 and compared to the SM  $t\bar{t}$  parton level predictions obtained from Powheg Monte Carlo.

We observe reasonable agreement between the observed yields and the predictions from MC and data-driven background estimates. We therefore do not observe evidence for an excess of events above SM expectations.

Table 19: Asymmetry variations due to  $t\bar{t}$  modeling.

Asymmetry variations	
Lepton charge	0.001
Lepton azimuthal angle	0.000
Top charge	0.003
Top polarization	0.030
Top spin correlation	0.037

Table 20: Summary of the measured asymmetry values (with statistical uncertainties only).

Variable	Data	Powheg
$A_{lepC}$	$0.01 \pm 0.01$	$-0.002 \pm 0.002$
$A_{\Delta\phi}$	$-0.10 \pm 0.01$	$-0.120 \pm 0.002$
$A_{topFB}$	$-0.009 \pm 0.023$	$0.005 \pm 0.002$
$P_n$	$-0.031 \pm 0.019$	$0.005 \pm 0.002$
$A_{c1c2}$	$-0.015 \pm 0.023$	$-0.061 \pm 0.002$

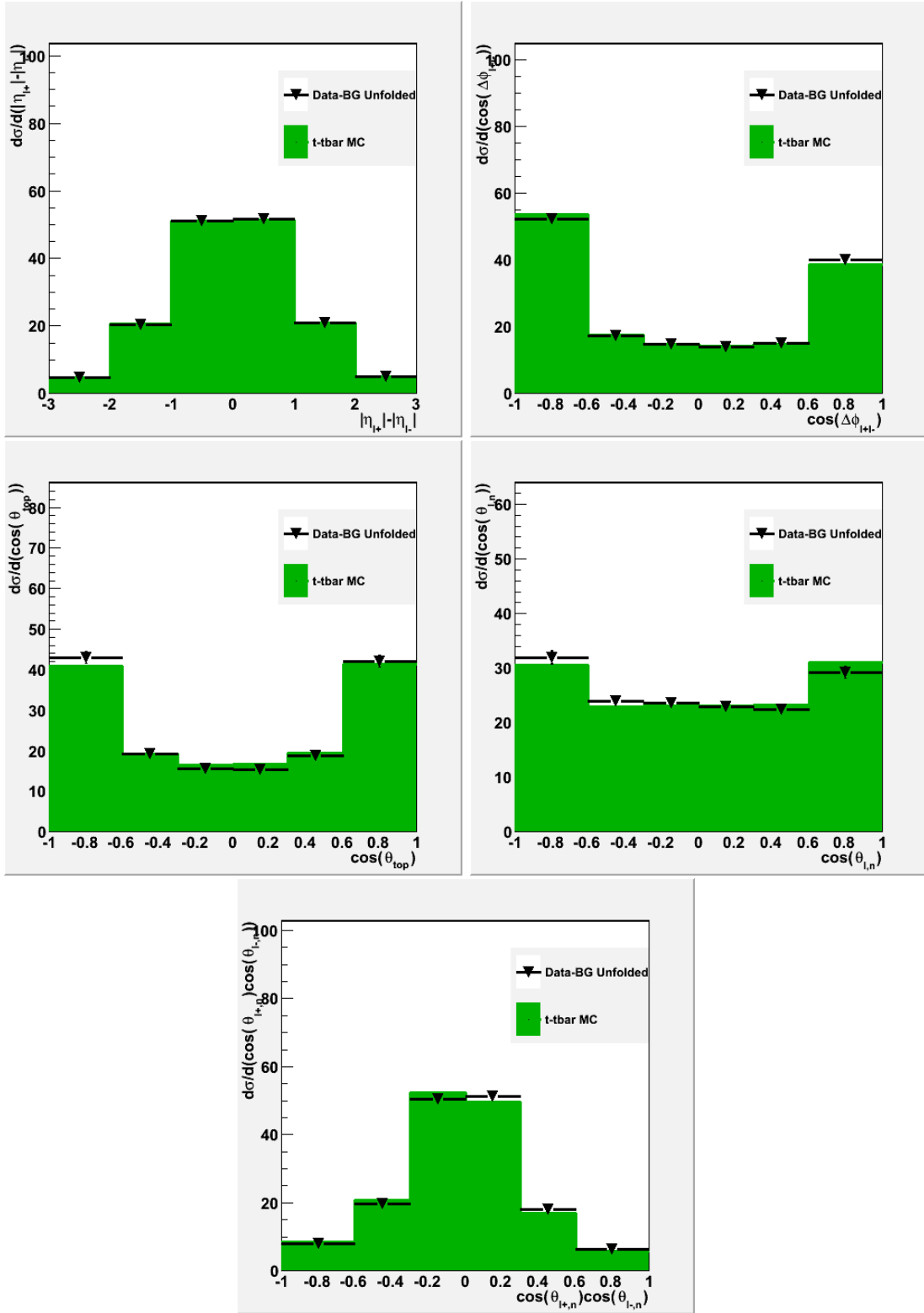


Figure 14: Background-subtracted and unfolded asymmetry distributions for the five variables of interest.

## References

- 375 [1] T. Aaltonen *et al.*, [CDF Collaboration], “Forward-Backward Asymmetry in Top Quark Production  
376 in  $p\bar{p}$  Collisions at  $\sqrt{s} = 1.96$  TeV,” Phys. Rev. Lett. **101**, 202001 (2008).
- 378 [2] V. Abazov *et al.*, [D0 Collaboration], “Measurement of the Forward-Backward Charge Asymmetry  
379 in Top-Quark Pair Production,” Phys. Rev. Lett. **100**, 142002 (2008).
- 380 [3] T. Aaltonen *et al.*, [CDF Collaboration], “Evidence for a Mass Dependent Forward-Backward Asym-  
381 metry in Top Quark Pair Production,” Phys. Rev. **D83**, 112003 (2011).
- 382 [4] D. Krohn, T. Liu, J. Shelton, and L.-T. Wang, “A Polarized View of the Top Asymmetry,” Phys.  
383 Rev. **D84**, 074034 (2011).
- 384 [5] P.H. Frampton, P.Q. Hung and M. Sher, Phys. Rept. 330 (2000).
- 385 [6] G.D. Kribs, Phys. Rev. D 76, 075016 (2007).
- 386 [7] W.-S. Hou, Chin. J. Phys. 47 (2009).
- 387 [8] B. Holdom *et al.*, PMC Phys. A 3 (2009).
- 388 [9] T. Aaltonen *et al.*, [The CDF Collaboration], Phys. Rev. Lett. **106**, 141803 (2011).
- 389 [10] J. Conway *et al.*, CDF public conference note CDF/PUB/TOP/PUBLIC/10110.
- 390 [11] D. Decamp *et al.*, Phys. Lett. B 231 (1989).
- 391 [12] E. L. Berger and Q. H. Cao, Phys. Rev. D **81**, 035006 (2010).
- 392 [13] O. Eberhardt, A. Lenz and J. Rohrwild, Phys. Rev. D **82**, 095006 (2010).
- 393 [14] Phys.Lett.B 695:424-443, 2011
- 394 [15] CMS Collaboration, “Performance of b-jet identification in CMS”, CMS PAS BTV-11-001, CMS  
395 PAS BTV-11-002, and CMS PAS BTV-11-003.
- 396 [16] CMS Collaboration, “A Higgs boson search in the fully leptonic  $W^+W^-$  final state with the full  
397 2011 dataset”, CMS AN- 2011/456’,
- 398 [17] <https://twiki.cern.ch/twiki/bin/viewauth/CMS/SimpleCutBasedEleID>
- 399 [18] D. Barge *at al.*, AN-CMS2009/159.
- 400 [19] W. Andrews *et al.*, AN-CMS2009/023.
- 401 [20] CMS Collaboration, “Search for new physics in events with opposite-sign dileptons and missing  
402 transverse energy”, CMS PAS SUS-11-011.
- 403 [21] <https://twiki.cern.ch/twiki/bin/view/CMS/ProductionReProcessingSpring10>
- 404 [22] D. Barge *at al.*, AN-CMS2010/257.
- 405 [23] CMS Collaboration, “Measurement of CMS luminosity”, CMS PAS EWK-10-004 (2010).
- 406 [24] CMS Collaboration, “Combination of top pair production cross section measurements”, CMS PAS  
407 TOP-11-024 (2011).
- 408 [25] M. Aliev *et al.*, HATHOR Hadronic Top and Heavy quarks cross section calculator, Comput. Phys.  
409 Commun. 182 (2011) 10341046.
- 410 [26] T. Junk, Confidence level computation for combining searches with small statistics, 362 Nucl. In-  
411 strum. Meth. A434 (1999) 435443, arXiv:hep-ex/9902006.
- 412 [27] A. L. Read, Presentation of search results: The CL(s) technique, J. Phys. G G28 (2002) 364 26932704.  
413 doi:10.1088/0954-3899/28/10/313.

## 414 **Appendix A Fakeable Object Definitions**

415 We estimate the contributions from leptons not originating from  $W/Z$  decay (fake leptons) using the  
416 data-driven fake rate method [14]. We define the following fakeable object selections, by taking the  
417 electron and muon requirements listed in Section 3 and loosening the following requirements:

418 • electrons

419 –  $d_0 < 0.2$  cm

420 –  $Iso \equiv E_T^{iso}/p_T < 0.4$ ,  $E_T^{iso}$  is defined as the sum of transverse energy/momentum deposits in  
421 ecal, hcal, and tracker, in a cone of 0.3. A 1 GeV pedestal is subtracted from the ecal energy  
422 deposition in the EB, however the ecal energy is never allowed to go negative.

423 • muons

424 –  $d_0 < 0.2$  cm

425 –  $\chi^2/\text{ndof}$  of global fit  $< 50$

426 –  $Iso \equiv E_T^{iso}/p_T < 0.4$ ,  $E_T^{iso}$  is defined as the sum of transverse energy/momentum deposits in  
427 ecal, hcal, and tracker, in a cone of 0.3.

## 428 **Appendix B Data and MC comparison for the preselection**

429 In this section we show plots that compare the data and MC distributions for several important variables.

430 Overall, the agreement is reasonable.

